Journal of
Synchrotron Radiation

ISSN 0909-0495

Received 10 February 2005
Accepted 12 April 2005

A new cell for the study of *in situ* chemical reactions using X-ray absorption spectroscopy

Alessandro Longo,[a]* Antonella Balerna,[b] Francesco d'Acapito,[c] Fabio D'Anca,[c] Francesco Giannici,[d] Leonarda F. Liotta,[a] Giuseppe Pantaleo[d] and Antonino Martorana[a,d]

[a]ISMN-CNR, Via Ugo La Malfa 153, 90146 Palermo, Italy, [b]Laboratori Nazionali di Frascati, Via E. Fermi 40, I-0004 Frascati, Italy , [c]OGG-INFM at ESRF, 6 rue Jules Horowitz, BP 220, 38043 Grenoble CEDEX 9, France, and [d]Universitá degli studi di Palermo, Dipartimento di Chimica Inorganica e Analitica 'Stanislao Cannizzaro', Parco D'Orleans padiglione 17, Viale delle Scienze, 90128 Palermo, Italy. E-mail: alex@pa.ismn.cnr.it

An *in situ* cell for reductive and oxidative treatments at different temperatures that allows the possibility of recording data as a function of temperature has been designed and constructed for X-ray absorption experiments at the GILDA beamline BM08 of ESRF. The cell is linked to a mass quadrupole spectrometer providing control of the reaction gases and monitoring of the products. The apparatus allows measurements to be performed both in transmission and fluorescence geometry. The cell was tested by studying the CO oxidation reaction promoted by a Pt/ceria-zirconia-supported catalyst. The CO_2 yield is correlated with the structural results confirming the existence of a strong metal–support interaction between the Pt metal clusters and the ceria-zirconia support.

Keywords: *in situ* EXAFS; three-way catalysts; strong metal support interaction.

1. Introduction

The possibility of performing time- and temperature-resolved experiments using *in situ* devices is one of the most important tools for studying catalysts or other materials and obtaining a deeper knowledge of the relationships between structure and properties. For this reason, many *in situ* cells have been designed and assembled; although each one has its own peculiarities (Pettiti *et al.*, 1999; Van Bokhoven *et al.*, 1999; Bando *et al.*, 2001; Wienold *et al.*, 2003; Lamberti *et al.*, 2003; Carlsson *et al.*, 2004; Huwe & Fröba, 2004), the main features of these devices are quite similar.

Recently, Huwe & Fröba (2004) presented a new *in situ* cell which allows XAFS (X-ray absorption fine structure) experiments to be performed at very high temperatures in transmission and fluorescence geometry over a wide energy range. Although by using this cell it is possible to carry out measurements at 1250 K, XAFS spectra cannot be recorded at temperatures lower than 298 K. In a previous paper, Pettiti and co-workers (Pettiti *et al.*, 1999) described a cell for catalytic applications both at high and at liquid-nitrogen temperatures, suitable for reducing and oxidizing reactions. With this apparatus, however, the control and the direct detection of the reaction gas mixtures is not allowed. In this paper, a new cell for *in situ* treatments is described. The cell can be operated in three different ways:

(i) After treatment at a suitable temperature and in a controlled chemical environment the sample is placed in an inert atmosphere, the temperature is lowered to that of liquid nitrogen and a static XAFS experiment is carried out.

(ii) Once the sample has reached a stationary state the XAFS experiment is performed, maintaining the attained temperature and chemical environment.

(iii) The XANES (X-ray absorption near-edge structures) part of the X-ray absorption spectrum can be collected in quick mode to follow structural/chemical changes of the sample during treatment.

As a test case, the structural analysis performed on a Pt/ceria-zirconia three-way catalyst is reported.

2. Set-up of the *in situ* cell

The new *in situ* cell reported in this paper has the following main features:

(i) The possibility to record XAFS spectra in both absorption and fluorescence mode is given.

(ii) XAFS spectra at low and high temperatures can be recorded.

(iii) Different gases can be introduced into the sample environment and monitored together with the products of the reduction and oxidation cycles using a mass spectrometer.

A schematic view of the cell is shown in Figs. 1 and 2. The cell is made up of two parts: a cylindrical steel (AISI321) vessel used as a thermal screen, and a sample holder directly welded to a cold and warm finger. The cylindrical steel vessel is equipped with three Kapton (100 µm-thick epoxy sealed

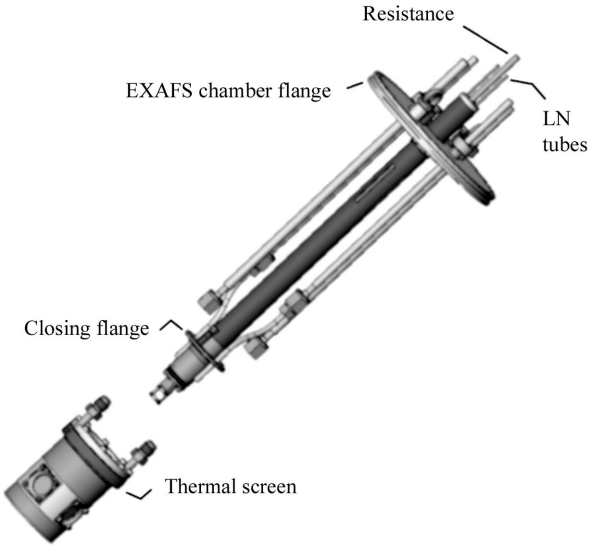

Figure 1
The two main parts of the *in situ* cell: thermal screen, and cold and warm finger.

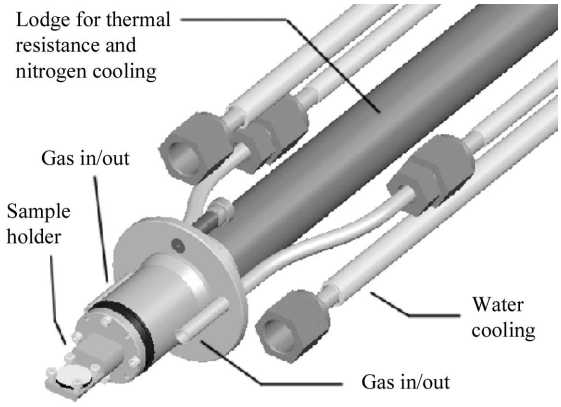

Figure 2
Sample holder of the *in situ* cell.

Kapton) windows, each of diameter 22 mm; the sample-to-window distance of 30 mm allows an angular aperture of 40° for the outcoming radiation. This configuration is particularly suited for transmission- and fluorescence-mode XAFS measurements, achieved by simply rotating the sample holder flange by 45°.

The cylindrical vessel is kept at room temperature by means of a cooling water circuit set within the cylindrical shelter. This feature avoids possible damage of the Kapton windows owing to thermal radiation emitted by the sample during the heating treatments.

The sample holder has two main parts. The first part is a gold-coated copper frame in which the sample is fitted. To improve its thermal contact, the sample is gently pressed using a clamp. A class K thermocouple inserted into the cell by a feedthrough crossing the closing flange, and suitably sited close to the sample holder, monitors the sample temperature and provides feedback to the thermoregulator.

The second part of the sample holder is a steel structure which contains the cold and the warm finger. Inside this element, a stainless-steel U-shaped tube is set for liquid-nitrogen flow during low-temperature measurements or, during thermal treatments, for nitrogen gas flow to avoid local overheating. The final parts of the U-shaped tube (external diameter = 2 mm) that cross the closing flange are connected to wider tubes (external diameter = 4 mm) with two Swagelok fittings. This system allows 173 K to be reached, as a lowest temperature. Finally, a suitable lodge of diameter 6.5 mm allows thermal contact between the sample holder and an electrical resistance. Therefore, heating of the sample during thermal treatments is achieved by heat conduction: the resistance used determines the highest attainable temperature, which cannot exceed 850 K. The sample can be changed simply by unscrewing the upper flange of the cell and lowering the cylindrical vessel.

Tubes for the inlet and outlet of the reaction gases pass through the top of the closing flange. The outlet tube is connected to a mass spectrometer (VGQ England). The gas flow can be set to the most suitable values for the investigated reaction by tuning a bottle manometer and a mass flow controller (Brooks Instrument; maximum flow: 104 ml min^{-1}).

The *in situ* cell can be easily installed in the experimental chamber. All the cooling tubes and heating devices are included in a DN160LF top flange by means of suitable feedthroughs. The x, z movements of the chamber then allow the perfect alignment of the sample to the beam position. The cell was tested for the effective temperature on the sample. Heating was carried out by raising the temperature of the electrical resistance and keeping the sample in a flow of He. The temperatures of the sample holder and of the sample were measured by thermocouples. The highest temperature reached on the sample was 773 K, while the corresponding temperature of the sample holder was 820 K. The temperature of the Kapton windows was about 308 K, while the lowest temperature on the sample was 173 K. For all of the tests the equilibrium temperature of the sample was reached in about 20 min.

During chemical reactions involving the sample lodged in the cell, the reaction products monitored by the mass spectrometer were analyzable and the reaction products and reaction kinetics were reproducible.

3. Test case: structural analysis of a Pt/ceria-zirconia catalyst

Three-way Pt/ceria-zirconia catalysts are employed for the exhaust treatment in gasoline-fuelled vehicles to achieve simultaneous control of CO, hydrocarbons and NO emission. Platinum promotes the oxidation of CO and hydrocarbons, while the ceria-zirconia support is able to store and release oxygen, owing to the easy reducibility of Ce^{IV} to Ce^{III} and *vice versa*. Reducible supports can give rise to the so-called strong metal–support interaction that originates peculiar catalytic properties in the supported metal phase (Tauster *et al.*, 1978). Recently, *in situ* X-ray diffraction (XRD) experiments

performed at the GILDA beamline (Martorana *et al.*, 2003, 2004) on Pt/ceria-zirconia catalysts allowed the structural modifications that take place in ceria-zirconia during the anaerobic CO oxidation reaction to be determined (Martorana *et al.*, 2004). Under these reaction conditions, the oxygen for CO oxidation is entirely provided by the support, through a mechanism involving the reduction of cerium. It was also shown that the structural kinetics of ceria-zirconia and of Pt/ceria-zirconia during reductions at 773 K are quite different, proving the presence of an effect owing to the metal–support interaction. However, it was not possible to gain other information because in the *in situ* XRD patterns the Pt phase was not detectable.

Therefore, in order to obtain detailed information on the chemical environment of Pt in the catalysts already studied, the XAFS measurements become fundamental. While several studies have been performed on ceria-based three-way catalysts at the Ce *K* or L_{III} edges (Fonda *et al.*, 1999), only a few deal with the Pt L_{III} absorption edge (Bitter *et al.*, 2000; Bera *et al.*, 2003) of Pt catalysts supported on pure ceria or ceria-zirconia. In these papers the most important evidence is that the strong metal–support interaction effects between Pt and ceria depend on the reduction treatment: at temperatures up to 773 K it produces a modification of the electronic structure of Pt, while at 973 K it determines the decoration of the metal phase with partially reduced ceria and Ce–Pt alloying. As shown, the metal phase plays a fundamental role in the behavior of the catalyst, and actually some of the unsolved fundamental aspects are the complete explanation of the mechanism leading to the reduction of the support, the study of the oxidation state of supported platinum and its behavior during the redox treatments. The results of XAFS experiments carried out in fluorescence geometry at GILDA by the *in situ* cell described in §2 are reported in the following section.

3.1. Sample treatments and XAFS measurements

The $Ce_{0.6}Zr_{0.4}O_2$ support was prepared by the sol–gel method according to a published procedure (Liotta *et al.*, 2003). 1 wt% Pt then was added by impregnating the support with a calculated amount of Pt(acetylacetonate)$_2$ solution in toluene at 343 K. After drying under vacuum, the solid was calcined at 673 K for 4 h in order to oxidize the organic ligands.

The XAFS experiments were carried out at the Pt L_3 edge (E_0 = 11565 eV) at the GILDA-CRG beamline of the European Synchrotron Radiation Facility (d'Acapito *et al.*, 1998). The monochromator was equipped with a pair of Si(311) crystals and was run in the so-called dynamical focusing mode (Pascarelli *et al.*, 1996). Harmonic rejection was achieved by using a pair of Pd-coated mirrors with an incidence angle of 3 mrad (E_{cutoff} = 21 keV). An ion chamber filled with Ar gas was used for normalization whereas the absorption coefficient of the sample was detected in fluorescence mode by using a 13-element high-purity Ge multidetector (MD) coupled to an X-ray pulse digital analyzer for more accurate correction of dead-time effects (Ciatto *et al.*, 2004). The MD resolution allowed selection of the Pt L_α fluorescence lines over the background originated by elastic, Compton and other fluorescence signals, improving the data quality. To reduce the total number of counts, which was very high owing to the fluorescence signals of the substrate, a 100 mm Al filter was placed in front of the MD (Pt L_α intensity reduction ∼30%). The spectra of the Pt catalyst were detected according to the procedure reported below and the reference samples were measured at 77 and 173 K.

For the *in situ* EXAFS measurements the platinum-supported catalysts were pressed into boron nitride pellets of diameter 10 mm and thickness 0.5 mm. Fig. 3 shows a typical fluorescence yield spectrum. The quality of the spectrum is good and allows an accurate data analysis. A preliminary test on the pellet consisted of sending a gas reaction mixture (0.5% CO in He, 100 ml min^{-1} flux) to the sample placed in the *in situ* cell at a temperature of 773 K. The reaction kinetics were recorded by monitoring the products and the reaction gases using the mass spectrometer. Fig. 4 reports typical CO_2 kinetics, obtained by flowing CO/He on the pellet made up of

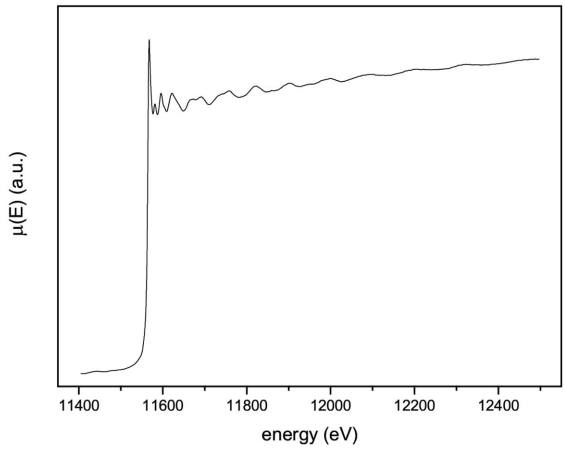

Figure 3
Fluorescence yield spectrum of a CO reduced catalyst collected using the *in situ* cell.

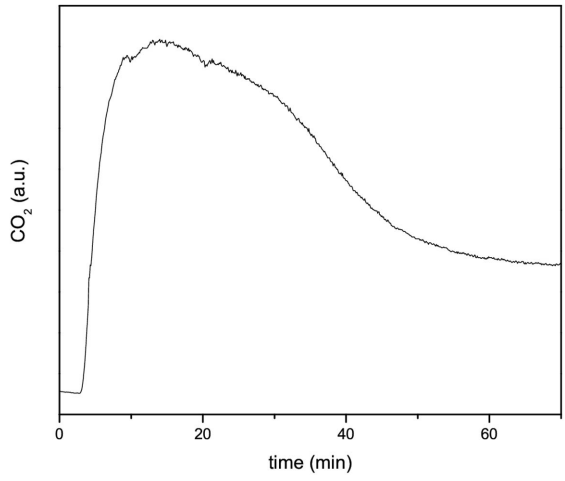

Figure 4
Typical kinetics of the CO_2 production at 773 K detected with the mass spectrometer during continuous CO/He flow.

Pt/ceria-zirconia mixed with boron nitride. Inspection of Fig. 4 shows that an induction time of about 2.5 min occurs between switching on the reaction gas (at time $t = 0$) and the onset of the CO_2 yield. This delay is due to the time necessary to permeate the overall volume of the reaction system, consisting of about 2.5 m of tubing and the reaction camera. Evidence of this estimate is provided by Fig. 5, reporting the CO_2 produced by flowing the reaction mixture for 5 min and performing mass spectrometer measurements for a further 15 min. By inspection, it is clear that the CO_2 production continues for about 2.5 min after the CO flow is interrupted, and then decays owing to complete consumption of the reagent.

The kinetics reported in Fig. 4 refer to the continuous flow of the reaction mixture CO/He until the CO_2 yield fades to an almost constant value. As oxygen is not flowed, the oxidation of CO is carried out by oxygen provided by the catalyst. The X-ray absorption experiments were performed in the 0–38 min interval. The upper limit corresponds to a decrease in the CO_2 production owing to the depletion of the oxygen that the catalytic system can provide. Thereafter, the CO_2 yield continues with a slow negative slope that can be partially attributed to a residual oxygen release and to the CO disproportionation reaction occurring at the surface of ceria-zirconia TWC systems (Holmgren & Andersson, 1998). Some minor differences with respect to the reaction kinetics reported in previous *in situ* XRD measurements (Martorana *et al.*, 2003, 2004) can be attributed to the different reaction conditions (flux, geometry *etc.*) in the two reactors; a deeper analysis will be discussed elsewhere.

We also verified, during these tests, that the cell is vacuum tight up to 0.1 Pa and that it can work at a pressure of about 2×10^5 to 2.5×10^5 Pa. Taking into account the kinetics profile reported in Fig. 4, after XAFS data collection on the as-prepared sample the following treatments and XAFS experiments were carried out:

(i) The sample was subjected to a CO/He (0.5 vol%, 100 ml min^{-1}) gas mixture flow for 15 min at 773 K, then the CO/He mixture was switched off and He was applied for 5 min at 773 K in order to stop the conversion of CO into CO_2; at this point an XAFS measurement at 173 K was recorded.

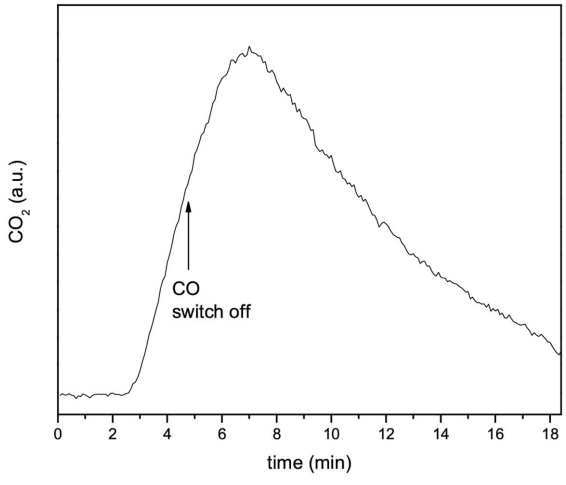

Figure 5
Kinetics of the CO_2 production at 773 K detected with the mass spectrometer during a 5 min CO flow. The switch-off time is indicated by the arrow.

Table 1
XAFS analysis fitting results of the catalysts after each reductive treatment.

Subscript 1 relates to the Pt–O contribution and subscript 2 to the metallic Pt–Pt contribution. The Debye–Waller factors (σ_i^2) are given $\times 10^{-3}$ Å^2. N is the coordination number. R_1 and R_2 are the first and the second shell distance, respectively, expressed in Å.

Treatment	N_1	R_1	σ_1^2	N_2	R_2	σ_2^2
As prepared	5.1 (8)	2.02 (1)	2 (1)	–	–	–
15 min	1.1 (6)	2.04 (6)	10 (8)	7 (2)	2.72 (2)	17 (3)
Re-oxidized	4.8 (7)	2.02 (1)	2 (1)	–	–	–
3 min	4.8 (7)	2.02 (1)	2 (1)	–	–	–
8 min	1.9 (9)	2.07 (8)	20 (8)	7 (2)	2.72 (1)	16 (2)
38 min	1.0 (8)	2.00 (8)	20 (8)	7 (1)	2.70 (1)	13 (2)

(ii) The sample was subjected to a 5 vol% O_2/He mixture flow (100 ml min^{-1}) at 773 K for 20 min to ensure its complete oxidation; then an XAFS spectrum was collected at 173 K.

(iii) Step (i) was repeated, changing the time scale. Instead of 15 min the chosen times were 3, 8 and 38 min, respectively. XAFS measurements at 173 K were performed after each reductive treatment.

Taking into account the first spectrum on the 'as-prepared' samples and the different redox treatments, six XAFS spectra were collected. The XAFS data were extracted using the *EDA* (Kuzmin, 1995) package of programs. Phase shifts and back-scattering amplitudes for the Pt–Pt and Pt–O scattering pairs, according to the ($Fm\bar{3}m$) and the ($P\bar{3}m1$) crystalline structures, were generated utilizing the *FEFF8* code (Ankudinov *et al.*, 1998). These phase shifts and backscattering amplitudes were calibrated with the help of the XAFS spectra of the Pt foil and platinum oxide. For the Pt foil, four shells were taken into account, together with the necessary multiple-scattering contributions. The analysis of the Pt foil at 173 K and 77 K, as expected, shows only a small difference in the Debye–Waller parameters. This suggests that 173 K is a reasonable temperature for performing XAFS experiments at the Pt L_{III} edge because it is low enough to reduce the anharmonic effects (Clausen & Norskov, 2000) and their influence on the XAFS structural information. The results achieved on the reference samples are in good agreement with the crystallographic parameters. S_0^2 was found to be equal to 1 for the Pt foil and 0.7 for platinum oxide.

For the analysis of platinum oxide and of the ceria-zirconia-supported Pt samples, two contributions were used: Pt–O for the first coordination shell and metallic Pt–Pt for the second. The results are reported in Table 1. Fig. 6 shows the calculated and experimental XAFS signals relative to the above-described treatments (upper panel) and to the reference samples (lower panel); the Fourier transforms of the XAFS signals are reported in Fig. 7 for the reference samples and in Fig. 8 for the treated samples. By inspection of Fig. 8, it is evident that for the 'as-prepared' catalyst and for the oxidized catalyst the only contribution needed to fit the data is that of Pt–O. Similar results were achieved for the samples treated

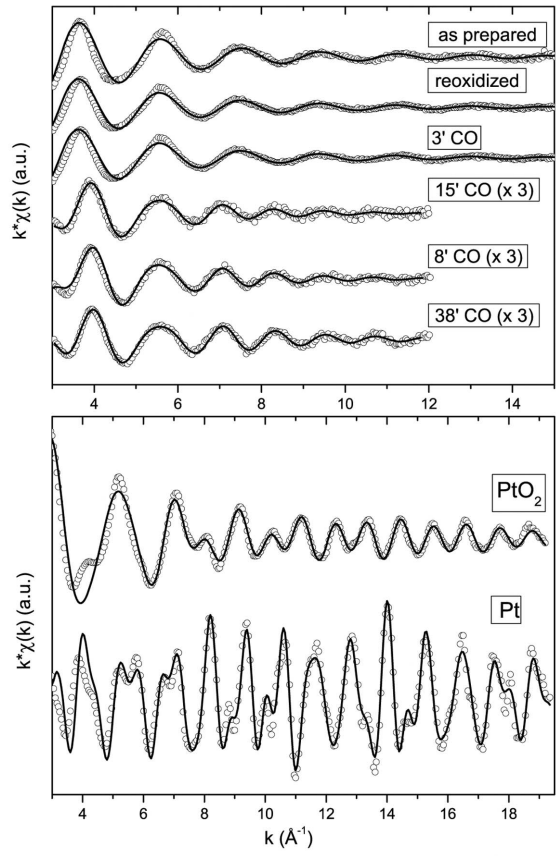

Figure 6
Experimental and calculated $k\chi(k)$. The upper panel shows the results relative to different reduction times of the Pt/ceria-zirconia catalyst. The lower panel shows the fitting of the Pt foil and Pt oxide.

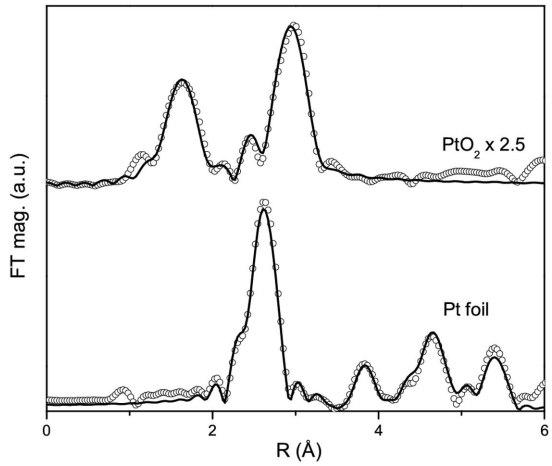

Figure 7
Experimental and calculated $k^3\chi(k)$ Fourier transforms relative to Pt foil and Pt oxide.

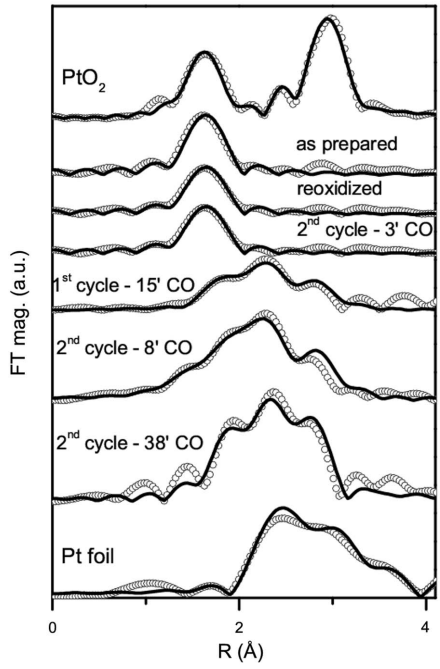

Figure 8
Experimental and calculated $k^3\chi(k)$ Fourier transforms relative to the Pt/ceria-zirconia catalyst at different reduction times. The Fourier transform was calculated in the same k-space interval for both standards and samples. The sample treated for 15 min is scaled by 0.5.

only for 3 min with the reductive CO/He mixture at 773 K. During the 3 min treatments the presence of CO_2 was detected by the mass spectrometer. This suggests that, since the reduction of Pt did not occur in these 3 min (see Table 1), the CO_2 detected by mass spectrometry is initially produced by the most accessible oxygen species, probably consisting of adsorbed atoms. When the reductive treatment is longer than 3 min, the reduction of Pt takes place. Actually, in fitting the data relative to the samples treated for 8 min, 15 min and 38 min with the CO/He at 773 K, the metallic Pt–Pt contribution together with the Pt–O must be included. It is notable that, after 38 min, CO_2 production is still detectable, suggesting that the complete reduction of the sample does not occur within this time, although the reduction of the metal clusters seems to stop after 15 min (see Table 1). The CO_2 yield after 15 min should therefore be attributed only to the ceria-zirconia oxygen and, for larger times, to the CO disproportionation reaction. Comparing the coordination numbers, no increase of the Pt cluster size is evident, although some minor difference can be attributed to the Pt–O correlation, more evident for the 15 min CO/He reduced sample. By inspection of Table 1, it can be seen that the contribution of Pt–O is still essential in the analysis of the sample treated for 38 min in CO/He at 773 K, as well as for the samples treated for 8 min and 15 min with the reductive mixture. Moreover, no difference in the coordination numbers was found in the Pt–Pt shell as a function of the reduction time.

Recently, Mullins & Zhang (2002) showed that an electronic interaction exists between the metallic Pt and the ceria-zirconia support when a reductive treatment is performed. Many recent papers (Bernal *et al.*, 1999; Miller *et al.*, 2000; Ramaker *et al.*, 2001; Mullins & Zhang, 2002) have proven that this interaction, called strong metal–support interaction (SMSI), induces a charge rearrangement between the Pt 6*s* orbitals within the metallic particles and the O atoms of the Pt–support interface, and *vice versa*, showing that the Pt atoms are in contact with the oxygen ions of the support (Bernal *et*

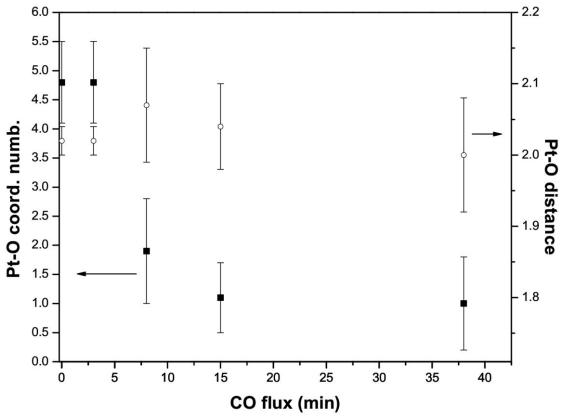

Figure 9
Variation of the coordination numbers (left-hand side) and first-shell interatomic distance (right-hand side) of the Pt catalyst as a function of the reductive treatment.

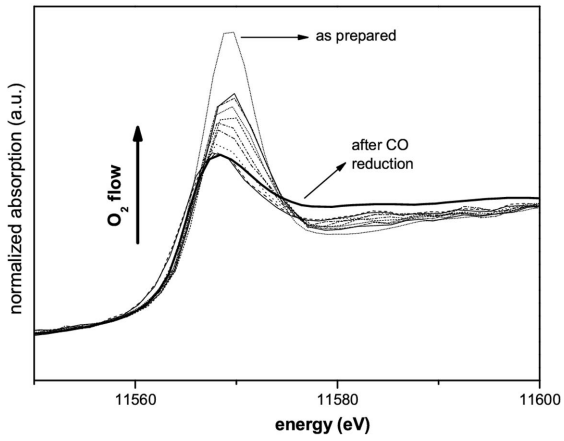

Figure 10
Quick-XANES spectra recorded during the re-oxidation of the reduced sample (O_2 5%/He at 773 K). Each spectrum is collected in 4 s and spectra were recorded every 20 s.

al., 1999; Miller *et al.*, 2000). In agreement with these previous results, we find that the Pt–O distance does not depend on the reduction time (see Fig. 9). In agreement with the constant values found for the coordination numbers, no increase of the clusters size occurs as the duration of chemical treatments at 773 K increases. This result is essentially due to the SMSI which prevents the sintering of the metal clusters (Bernal *et al.*, 1999), anchoring the metal particles to the ceria-zirconia surface. When the sample is re-oxidized, according to the literature on the SMSI effect, the SMSI breaks down and oxidation of the Pt clusters takes place (Tauster *et al.*, 1978). As reported in the *Introduction*, the *in situ* cell can also be used for the rapid collection of XANES spectra during the sample rearrangement produced by specific sample treatments. As an example, Fig. 10 reports the quick-XANES data recorded during the re-oxidation of a reduced sample. Each scan was collected in 4 s and different scans were collected every 20 s.

4. Conclusion

A new cell for *in situ* XAFS measurements linked to a mass quadrupole spectrometer has been designed and assembled. The cell works properly as a chemical reactor for kinetics studies and is very suited for high and low temperature as well as fluorescence and transmission XAFS measurements. In particular, the wide angular range for outcoming radiation allows the collection of high-quality fluorescence data. After preliminary tests carried out to check the actual temperature range of the sample, the CO oxidation reaction promoted by a Pt/ceria-zirconia-supported catalyst has been studied. Chemical and structural information were obtained and combined with the CO_2 yield monitored by mass quadrupole spectrometry. The results achieved are in agreement with literature data confirming the existence of the strong metal–support interaction between ceria-zirconia and platinum. As an improvement, changes in the set-up of the *in situ* cell are planned in order to perform time-resolved Q-EXAFS at the GILDA beamline.

Dr C. Maurizio is acknowledged for helpful discussions and F. La Manna for his technical contribution. The authors acknowledge for partial financial support the Ministero dell'Università e della Ricerca Scientifica e Tecnologica and the Consiglio Nazionale delle Ricerche. CNR, INFN, INFM institution are acknowledged for their financial support of the GILDA beamline.

References

d'Acapito, F., Colonna, S., Pascarelli, S., Antonioli, G., Balerna, A., Bazzini, A., Boscherini, F., Campolungo, F., Chini, G., Dalba G., Davoli, I., Fornasini, P., Graziola, R., Licheri, G., Meneghini, C., Rocca, F., Sangiorgio, L., Sciarra, V., Tullio, V. & Mobilio, S. (1998). *ESRF Newsl.* **30**, 42–44.
Ankudinov, A., Ravel, B., Rehr, J. J. & Conradson, S. D. (1998). *Phys. Rev. B*, **58**, 7565–7576.
Bando, K. K., Saito, T., Sato, K., Tanaka, T., Dumeignil, F., Imamura, M., Matsubayashi, N. & Shimada, H. (2001). *J. Synchrotron Rad.* **8**, 581–583.
Bera, P., Priolkar, K. R., Gayen, A., Sarode, P. R., Hegde, M. S., Emura, S., Kumashiro, R., Jayaram, V. & Subbanna, G. N. (2003). *Chem. Mater.* **15**, 2049–2060.
Bernal, S., Calvino, J. J., Cauqui, M. A., Gatica, J. M., Larese, C., Pérez Omil, J. A. & Pintado, J. M. (1999). *Catal. Today*, **50**, 175–206.
Bitter, J. H., Cauqui, M. A., Gatica, J. M., Bernal, S., Ramaker, D. E. & Koningsberger, D. C. (2000). *Stud. Surf. Sci. Catal.* **130**, 3183–3188.
Carlsson, P., Österlund, L., Peter Thormählen, P., Palmqvist, A., Fridell, E., Jansson, J. & Skoglundh, M. (2004) *J. Catal.* **226**, 422–434.
Ciatto, G., d'Acapito, F., Boscherini F. & Mobilio, S. (2004). *J. Synchrotron Rad.* **11**, 278–283.
Clausen, B. S. & Norskov, J. K. (2000). *Top. Catal.* **10**, 221–230.
Fonda, E., Andreatta, D., Colavita, P. E. & Vlaic, G. (1999). *J. Synchrotron Rad.* **6**, 34–42.
Holmgren, A. & Andersson, B. (1998). *J. Catal.* **178**, 14–25.
Huwe, H. & Fröba, M. (2004). *J. Synchrotron Rad.* **11**, 363–365.
Kuzmin, A. (1995). *Physica B*, **208/209**, 175–176.
Lamberti, C., Prestipino, C., Bordiga, S., Berlier, G., Spoto, G., Zecchina, A., Laloni, A., La Manna, F., D'Anca, F., Felici, R., d'Acapito, F. & Roy, P. (2003). *Nucl. Instrum. Methods Phys. Res. B*, **200**, 196–201.
Liotta, L. F., Macaluso, A., Longo, A., Pantaleo, G., Martorana, A. & Deganello, G. (2003). *Appl. Catal. A*, **240**, 295–307.

Martorana, A., Deganello, G., Longo, A., Deganello, F., Liotta, L., Macaluso., A., Pantaleo, G., Balerna, A., Meneghini, C. & Mobilio, S. (2003). *J. Synchrotron Rad.* **10**, 177–182.
Martorana, A., Deganello, G., Longo, A., Deganello, F., Liotta, L., Macaluso, A., Pantaleo, G., Balerna, A., Prestianni, A. & Mobilio, S. (2004). *J. Solid State Chem.* **177**, 1268–1275.
Miller, J., Mojet, B. L., Ramaker, D. E. & Koningsberger, D. C. (2000). *Catal. Today*, **62**, 101–114.
Mullins, D. R. & Zhang, K. Z. (2002). *Surf. Sci.* **513**, 163–173.
Pascarelli, S., Boscherini, F., d'Acapito, F., Hrdy, J., Meneghini, C. & Mobilio, S. (1996). *J. Synchrotron Rad.* **3**, 147–155.
Pettiti, I., Gazzoli, D., Inversi, M., Valigi, M., De Rossi, S., Ferraris, G., Porta, P. & Colonna, S. (1999). *J. Synchrotron Rad.* **6**, 1120–1124.
Ramaker, D. E., De Graaf, J., Van Veen, J. A. R. & Koningsberger, D. C. (2001). *J. Catal.* **203**, 7–17.
Tauster, S. J., Fung, S. C. & Garten, R. L. (1978). *J. Am. Chem. Soc.* **100**, 170–175.
Van Bokhoven, J. A., Van der Eerden, M. J., Smith, A. D. & Koningsberger, D. C. (1999). *J. Synchrotron Rad.* **6**, 201–203.
Wienold, J., Timpe, O. & Ressler, T. (2003) *Chem. Eur. J.* **9**, 6007–6017.